A bio-inspired single photon detector with suppressed noise and low jitter

Memis, Omer Gokalp, Katsnelson, Alex, Mohseni, Hooman, Yan, Minjun, Zhang, Shuang, et al.

Omer Gokalp Memis, Alex Katsnelson, Hooman Mohseni, Minjun Yan, Shuang Zhang, Tim Hossain, Niu Jin, Ilesanmi Adesida, "A bio-inspired single photon detector with suppressed noise and low jitter," Proc. SPIE 7035, Biosensing, 70350V (29 August 2008); doi: 10.1117/12.796448

Event: NanoScience + Engineering, 2008, San Diego, California, United States

A Bio-inspired Single Photon Detector with Suppressed Noise and Low Jitter

Omer Gokalp Memis[a], Alex Katsnelson[a], Hooman Mohseni[a*],
Minjun Yan[b], Shuang Zhang[b], Tim Hossain[b], Niu Jin[b], Ilesanmi Adesida[b]

[a]Bio-Inspired Sensors and Optoelectronics Laboratory, Northwestern University,
2145 Sheridan Rd, Evanston, IL, USA 60208;
[b]University of Illinois at Urbana Champaign, 208 N. Wright St, Urbana, IL USA 61801

ABSTRACT

A novel short wave infrared single photon detector was conceived for wavelengths beyond 1 μm. The detector, called the nano-injection photon detector, is conceptually designed with biological inspirations taken from the eye. Based on a detection process similar to the human visual system, the detector couples a nano-scale sensory region with a large absorption volume to provide a low-noise internal amplification mechanism, high signal-to-noise ratio and quantum efficiency. Tens of thousands of devices were fabricated in different configurations with conventional processing methods in more than 20 iterations. For low speed imaging applications, the detectors have shown gain values reaching 10,000 with bias voltages around 1 V. Ultra-low noise levels were measured at gain values exceeding 4,000 at room temperature: Fano factors as low as 0.55 has been achieved, which indicated a statistically stable amplification mechanism and resulting sub-Poissionian shot noise. An alternate version of the detector, which is specialized towards high-speed applications, has also been developed with slight changes in processing steps. The fast detectors with bandwidth beyond 3 Ghz were demonstrated which provide gain values around 20. The measured risetime was less than 200 ps. Femtosecond pulsed illumination measurements exhibited ultra-low jitter around 15 ps. Transient delay experiments revealed that the measured jitter is due to the transit time in the large absorption region. Hence the amplification process has insignificant time-uncertainty in addition to low amplitude-variance (noise), which is consistent with statistically stable nature of amplification.

Keywords: bio-inspired, single photon detector, infrared imagers, short-wave infrared, suppressed noise, Fano factor, jitter.

1. INTRODUCTION

Short-wave infrared (SWIR) photon detection has become an essential technology in modern world. For imaging purposes, this band provides a lot of benefits over the conventional visible imaging. Here in this paper, we present our findings of and results from bio-inspired nano-injection photon detectors suited to address some inherent issues of current SWIR imaging arrays towards SWIR imaging arrays.

Short-wave infrared spectrums spans from 1 μm to 3 μm wavelength[1]. In imaging applications, this spectrum presents important advantages, such as compatibility with glass optics, eye-safe operation[2], the ability to utilize intense night-glow[3]and/or complement visible or near-infrared spectrum for hyperspectral information[4].

In order to harness the powerful capabilities of short wave infrared, sensitive, efficient and versatile imagers are required. To become on par with visible and NIR imagers, the imagers also need to be primarily sensitive, but also small, cheap and high resolution. Sensitivity is of utmost importance, as low signal strength can cause artifacts in the image quality when coupled with the noise of the read-out integrated circuitry (ROIC) and other downstream noise sources. The sensitivity of a photodetector is closely related to some parameters: pixel size, individual quantum efficiency, array fill factor and operating temperature. Among these factors pixel size presents an important limitation. Larger pixel sizes give more signal-to-noise ratio (SNR), however they also increase the size and the cost of fabrication on device level.

* hmohseni@eecs.northwestern.edu; phone 1 847 491 7108; fax 1 847 491 4455; www.bisol.northwestern.edu

Biosensing, edited by Manijeh Razeghi, Hooman Mohseni
Proc. of SPIE Vol. 7035, 70350V, (2008) · 0277-786X/08/$18 · doi: 10.1117/12.796448

Furthermore, they strongly increase volume and weight in systems level, almost with the third power of pixel size, as they require bigger and bulkier optics[5]. In contrast, smaller pixel sizes do not suffer from any of these problems, and offer higher resolution arrays. Small pixel sizes can be hard to realize in conventional planar diffusion imagers[6], where pixel size can be limited by diffusion length. Reducing the pixel size makes the detectors more susceptible to cross-talk problems[7] in dense arrays. Besides pixel size, the device quantum efficiency and array fill factor are important parameters. They define the efficiency of light absorption and for efficient, high-fidelity detection down to single photon levels, a high fill factor is very desirable. Another important consideration for detector arrays is the operating temperature, which affects the size, cost and reliability of the imager. Operating temperatures requiring cryogenic cooling are significantly larger (up to 100 times), more expensive to operate and more susceptible to cooler problems compared to thermoelectric cooling[8].

In passive broadband imaging systems, where homo/heterodyning and coherent detection are not possible, semiconductor based detectors are favored due to the robustness, modest requirements and small footprints. Currently, PIN detectors, avalanche photodetectors (APDs) and superconducting detectors are utilized in infrared detection systems. PIN detectors are small devices with high-speed response and ultra-low jitter[9]. The have extremely low dark current values; however, PIN detectors do not provide internal amplification and are usually paired with electronic preamplifiers. Avalanche photodetectors, in contrast, are built around an internal multiplication scheme coupled to the detection mechanism[10]. APDs based on InGaAs/InP have been commonly used in near infrared spectrum and they provide stable gain values of less than two hundred at room temperature[11]. However, due to their internal positive feedback in avalanche multiplication, the gain tends to destabilize at higher values and increases amplitude uncertainty (i.e. noise) [12]. Finally, superconductor based single photon detectors (SSPD) usually exhibit very high amplification, low noise levels and high-speed operation, and they are usually operated at temperatures below 10 K[13].

Here in this paper, we will provide an overview of the nano-injection detector, involving detailed results and underlying physics. The detector was designed to overcome the limitations of existing detectors. Our initial reports about the nano-injection photon detector showed high gain values along with low dark current values[14]. Further investigations revealed that the noise levels measured at these high gain values were lower than the expected levels and we investigated this behavior and the reasons[15]. We have also produced surface passivated versions of the nano-injection detector, which showed high-speed response with reduced gain values (~10). The fast nano-injection detector exhibited a remarkably low jitter at room temperature[16]. More experiments were performed to explore the transient behavior more and measurements revealed the strong connection between lateral charge transfer process and jitter.

2. DEVICE DESIGN AND STRUCTURE

In parallel to the development of these existing single photon detectors, we started to seek a novel method of single photon detection. We have looked into nature itself to guide us, and tried to understand and replicate the basic mechanism of dim light vision. Human eye is surprisingly sensitive and is capable of detecting a few photons[17]. Rod cells that are responsible for such sensitivity[18] are made of inner and outer segments, among which a steady current flow due to Na+ and K+ transport in dark. Fig. 1-a shows the overall detection mechanism in the rod cells schematically. Outer segment is very rich in photosensitive rhodopsin molecule, which is a strong absorber of photons with peak sensitivity in blue-green spectrum. Upon light reception rhodopsin is triggered with structural changes and acts as a catalyst (Fig. 1-b) Activated rhodopsin triggers a chain of reactions that lead to the destruction of chemical messenger cyclic guanosine monophosphate (cGMP). Finally, the transport channels for Na+ and K+ respond quickly to any change in cGMP concentration by closing the ion channels, and significantly changing the current passing through the rod cell. The significance of this detection mechanism is that it can provide both high efficiency and high sensitivity at room temperature; a condition that is very difficult to achieve in conventional single photon detectors. Simply put, the energy of a single photon in the visible or short infrared is extremely small, less than one atto Joule, and the only reliable way of sensing this small energy is to use a very small sensing volume, for example a quantum dot. However, the wavelength of light is significantly larger than such a sensor, and hence the interaction between the photon and the sensor, or quantum efficiency, is extremely small. Any attempt to enhance the efficiency by increasing the volume would simply reduce the sensitivity. Rod cell's detection mechanism resolves this conflict by using a micrometer-scale absorbing volume, the outer cell, and nano-scale sensing elements, or the ion channels.

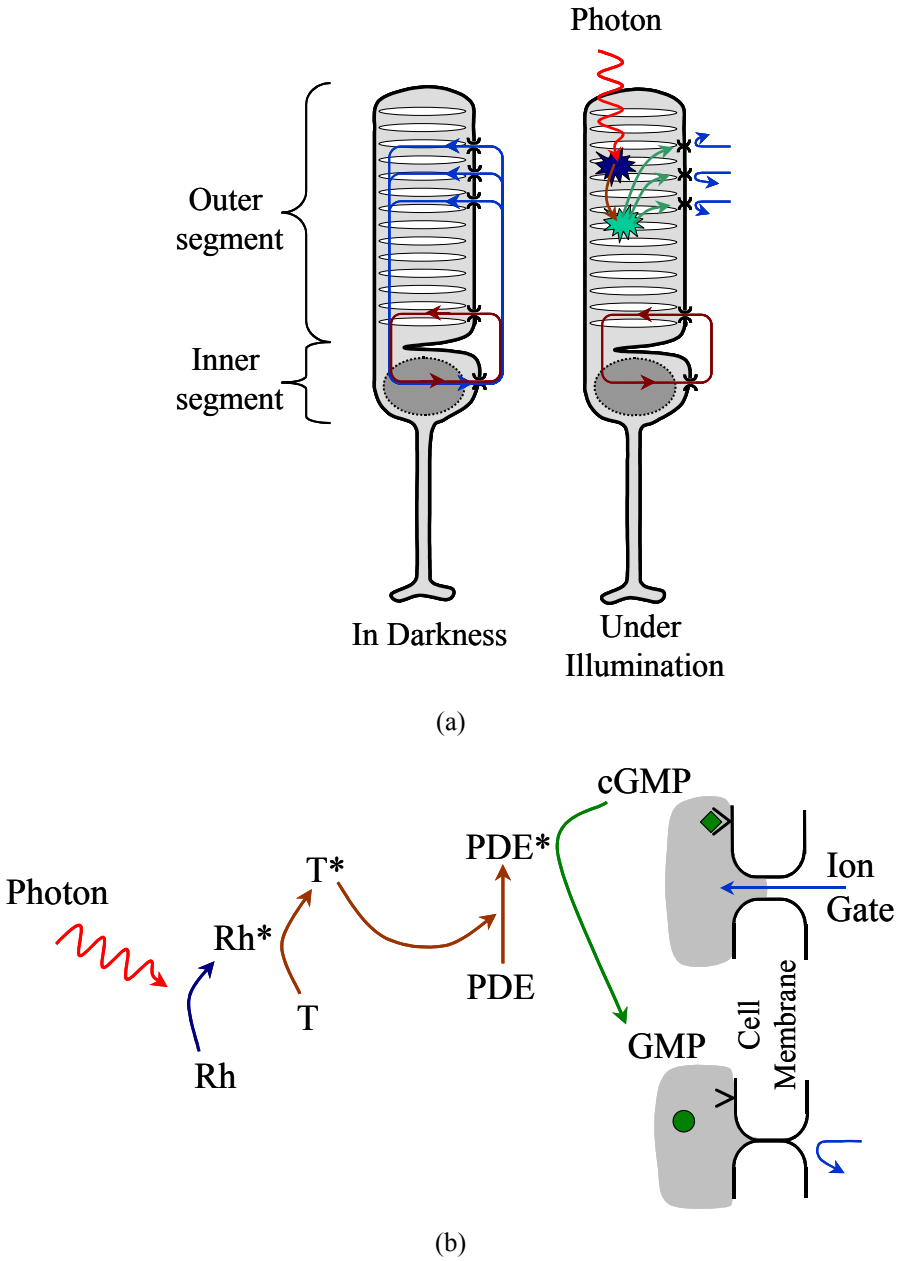

Fig. 1. The detector concept inspired by the detection mechanism in rod cells. (a) Photon detection process in the rod cells involves light absorption in a micron-scale absorbing volume, the outer cell, and nano-scale sensing elements, or the ion channels: (b) Upon light reception rhodopsin (Rh) is triggered with structural changes and starts acting as a catalyst. Activated rhodopsin (Rh*) consequently catalyzes Transducin (T→T*) which in turn interacts with and changes phosphodiesterase (PDE→PDE*) This chain reaction leads to the destruction of the chemical messanger cyclic guanosine monophosphate (cGMP). The transport channels for Na+ and K+ respond quickly to any change in cGMP concentration by closing the ion channels, significantly altering the current passing through the rod cell.

We incorporated similar principles in a novel semiconductor platform, called the nano-injection photon detector. The detector features large regions which absorb and channel the photo-excited carriers to nano-injectors which control the amplified flow of carriers, functioning similar to ion gates in rod cells.

The structure and mechanism of photon detection in the nano-injection photon detector is highlighted in Fig. 2. The detector features nano-injectors on a large InGaAs absorption layer. Looking at the central cross section of a single device, the material system n-InP/p-GaAsSb/n-InGaAs provides a type-II band alignment. Due to the doping level of each layer, the device generates an internal electric field in InGaAs region, which gets stronger when the device is biased correctly. When a photon is absorbed in InGaAs layer, the hole is attracted towards toe nano-injector due to this electric field. When the hole arrives at GaAsSb layer, the valance band structure of this material system with type-II band alignment ensures that the hole gets trapped inside. Furthermore, the volume of GaAsSb region is small, and this increases the change in GaAsSb potential due to the hole. To compare, the charge density due to a hole in InGaAs layer is around 10^{-3} C/m^3, whereas it increases to 400 C/m^3 in a nano-injector of radius 50 nm and thickness 50 nm.

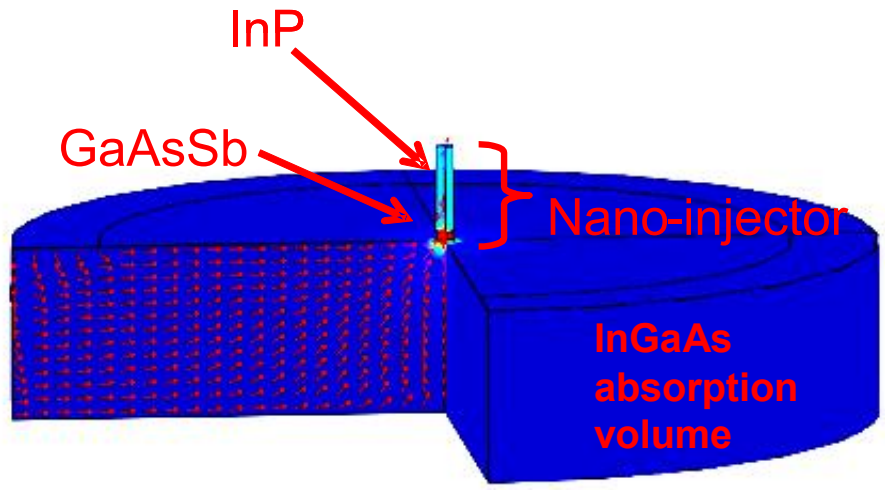

(a)

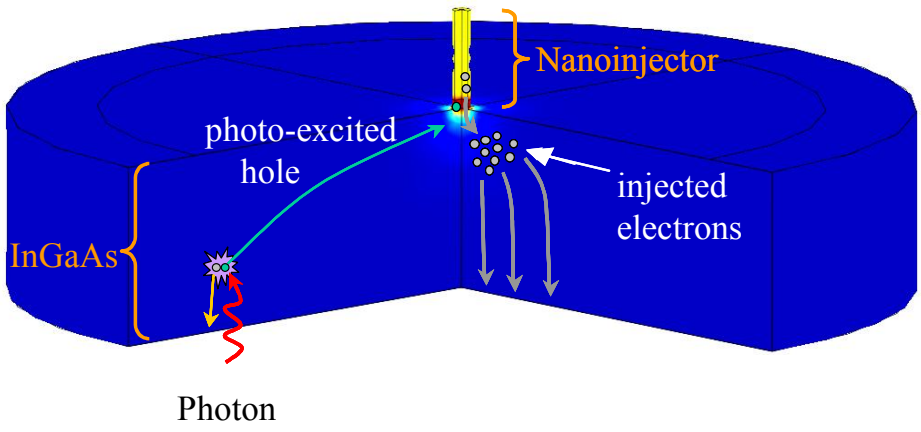

(b)

Fig. 2. (a) The detector features nano-injector pillars on top of large absorption volumes. (b) The large InGaAs regions absorb and channel the photo-excited carriers towards InP/GaAsSb nano-injectors, which control the amplified flow of injected carriers – electrons.

We used a custom developed three-dimensional simulation tool to design the epitaxial layer thickness, doping level, and composition. Epitaxial layers were grown by metal-organic chemical vapor deposition (MOCVD) on 2-inch InP substrates. The layer thickness of active layers from bottom to top was 1000 nm $In_{0.53}Ga_{0.47}As$, 50 nm $GaAs_{0.52}Sb_{0.48}$ and 500 nm of InP. In between the GaAsSb and InP regions, a 50 nm InAlAs layer was placed as an etch stop layer. Wafers were patterned with e-beam lithography to form different size pillars ranging from 100 nm to 15 μm diameters. The process consisted of dry etching with CH_4/H_2 in a reactive ion etcher to get unpassivated samples. Part of these samples was then planarized with polyimide to help form reliable top contacts to the sub-micrometer features. Conventional metallization with an e-beam evaporator was used to form the multi-layer metal contacts.

3. EXPERIMENTAL RESULTS

3.1 Devices with unpassivated surfaces

Fabricated devices were tested using a computerized setup, which has full automation capabilities for various measurement tasks including dark current, calibrated photocurrent, noise and time resolved high speed measurements. Various samples, which had undergone different processing steps, were tested in this custom setup for a variety of characterization parameters. The measured dark current values of unpassivated devices showed good agreement with the simulation results, without any fitting of simulation parameters. Dark current values of 1-2 μA were measured at 1 V in large devices (~30 μm) with 10 μm injectors. Smaller devices with 500 nm nano-injectors had less than 45 nA of dark current. For laser power calibration, a commercial PIN detector was placed inside the setup as a separate experiment and its response was measured to accurately quantify the laser power reaching the sample. Using calibrated photocurrent measurements, the "optical-electrical conversion factor", which is defined as the ratio of injected electrons to absorbed photons, was recorded and analyzed. This optical-electrical conversion factor, which is also the product of the electrical gain M and hole collection efficiency η_c, is chosen instead of the electrical gain since the detection and multiplication mechanisms are tightly coupled in our detector. It is important to note that, due to less than ideal collection efficiency, the optical-electrical conversion factor is always lower than electrical gain.

The optical-electrical conversion factor showed a monotonic increase with increasing bias voltage, and tended to stabilize at higher voltages. Beyond 1 V a stable gain of more than ten thousand was measured in large devices with 10 μm diameter injectors, and a gain of a thousand for smaller devices with 500 nm nano-injector. The devices exhibited very good tolerance to variations in voltage bias, as indicated by the flat gain-bias relation. Combining the dark current and gain measurements yielded a room temperature unity gain dark current density of less than 900 nA/cm^2 at 1 V.

The measured bandwidth of the unpassivated devices was around 3-4 kHz, much different compared to the lifetime in the GaAsSb trap layer (~1 nanosecond with our doping levels), which we believe will be the ultimate constraint on bandwidth. We have attributed this difference to the existence of surface traps with long recombination lifetime.

The spatial response of the unpassivated devices was measured using a surface scanning beam with ~1.5 μm diameter, and 10 nm step resolution. Despite such a high gain the devices show a very uniform spatial response that extends to approximately 8 μm away from the nano-injector. Beyond that, the response decreases quickly, which agrees with simulation results. This property suggests that two-dimensional arrays of such detectors might not necessarily need pixel isolation methods such as ion implantation or mesa etching as each pixel is self-contained.

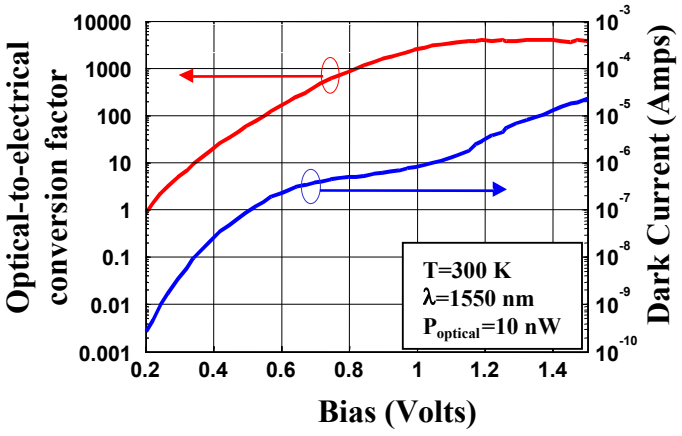

(a)

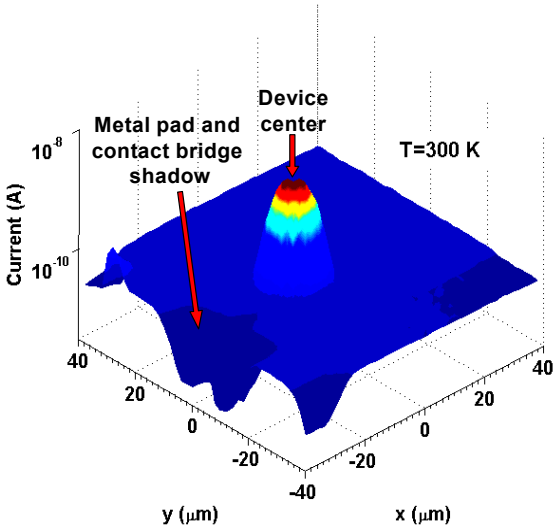

(b)

Fig. 3. (a) The dark current and optical-electrical conversion factor of a 10 μm injector device. (b) The spatial sensitivity map of the device. The detector exhibits an active area extending to 7-8 μm beyond the injector.

3.2 Noise measurements

Focusing on the relation between noise levels and amplification, it is important to quantify the noise levels and define figures of merit. To quantify the noise behavior, the excess noise factor F and fano factor γ have been introduced in two different contexts. They are both defined using the ratio of the measured shot noise to the expected noise.

Avalanche gain has been shown to possess a certain statistical variance due to the unpredictable nature of collisions and ionizations involved. The time-evolution of avalanche multiplication is a random variable in a statistical process which results in different amplification values for each carrier and elevated uncertainty. The excess noise factor F is used as the merit of noise performance in APDs, and is defined as[19]

$$F = \frac{I_n^2}{2qM^2 I_{\text{int}} \Delta f}$$

where I_n is the standard deviation of current, or current noise; q is electron charge; M is the multiplication factor or gain; I_{int} is the average value of current before it undergoes multiplication; and Δf is the bandwidth. Measurements on traditional InGaAs/InP based APDs show a monotonic increase in excess noise factor with increasing gain[12].

In contrast to the excess noise factor, the Fano factor is traditionally used in devices with sub-Poissonian (suppressed) shot noise. This suppression behavior is called the Fano effect, and it can stem from temporal correlations of carriers, which can be due to Pauli exclusion principle or Coulomb blockade. The Fano factor γ is

$$\gamma = \frac{I_n^2}{I_{shot}^2} = \frac{I_n^2}{2qI_{DC}\Delta f}$$

where I_n is the measured standard deviation of current, or current noise; I_{shot} is the Poissonian shot noise; q is electron charge; I_{DC} is the average value of current; and Δf is the bandwidth. Shot noise suppression with Fano factors around 0.4 has been demonstrated[20].

For accurate noise measurements, we simultaneously measured the dark current, photo-response and spectral noise power of the devices at room temperature. The devices were illuminated with a 1550 nm laser and they were probed with a shielded high-bandwidth. The signal was amplified using a trans-impedance amplifier and recorded by a high accuracy multimeter and a spectrum analyzer. Similar to reference 19, the spectral noise power after amplification was measured with a spectrum analyzer. The measurement was performed around 1.5 kHz, which is beyond the 1/f noise knee but lower than the measured bandwidth of the device. The measured spectral power was compared to predicted spectral noise density due to Poissonian shot noise with multiplication ($2qM2I_{int}\Delta f$). From the ratio of measured to expected noise powers, the Fano factor was calculated.

We have observed significant shot noise suppression in our devices[15]. The Fano factor was recorded as F~0.55 at optical-electrical conversion factors around 5,000. As the convention of optical-electrical conversion factor was used instead of electrical gain, the multiplication factor was constantly underestimated. This is a conservative approach, as overestimation of electrical-optical conversion factor would always lead to an overestimation of (or upper bound for) the Fano factor. For instance, assuming a collection efficiency of 70%, increase the gain to more than 7,000 and yields a Fano factor around 0.39, which would mean the Poissonian shot noise is further suppressed in reality. However, it was also observed that using optical-electrical conversion factor as electrical gain becomes a poor assumption at high optical intensities. As the incident optical power was increased, the measurements showed an overall decrease in optical-electrical conversion factor, which is a result of decreasing collection efficiency. We attribute the low collection efficiency to carrier shielding and device saturation at high optical intensities. As the holes are collected from the large absorption region and drawn into the small GaAsSb volume, the hole current density shows a rapid increase in the radial direction towards the center. The high density of holes at the center of the device repels the incoming hole flux through Coulomb forces and introduces carrier shielding. The collection efficiency η_c drops more as the carrier shielding becomes more pronounced at stronger illumination. The effect of lowered collection efficiency manifests itself as low optical-electrical conversion factors and an overall increase in Fano factor at high intensities. The noise equivalent power (NEP) of the devices was also measured, which was 4.5 fW/Hz$^{0.5}$ at room temperature without any gating.

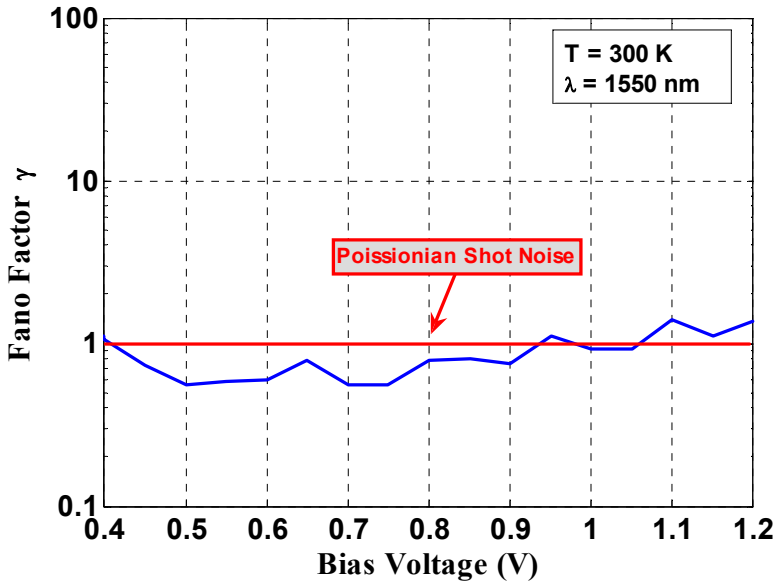

Fig. 4. The Fano factor versus bias plot of a device with 10 μm injector size. In the plot, the red line shows the expected Poissonian shot noise, which corresponds to a Fano factor γ of 1. The measured noise levels were lower than the Poissonian shot noise level, indicating the suppression of shot noise.

3.3 Surface Passivation

When the devices were passivated, we have observed a drastically different behavior. The gain decreased significantly to values around 10 and the spatial response extended to beyond 100 μm when the devices were not confined by hard-etching the trap layer. However, the bandwidth of these devices exceeded 3 GHz. The risetime values of 200 ps were measured. Further simulations confirmed that the InAlAs layer had more influence in passivated devices than unpassivated ones, and that it was responsible for the observed behavior. Simulation results showed great agreement in dark current and gain values.

The passivated devices showed very high uniformity across the arrays. The measurements in arrays of devices revealed highly uniform arrays with less than 3% standard deviation in dark current. We believe that the low internal electric field and the internal negative feedback in our devices are the main reasons for the observed spatial and statistical uniformity.

For transient response measurements on passivated devices[16], samples were illuminated with a femtosecond laser at 1.55 μm, with 300 fs pulse width and 20 MHz repetition rate. Calibrated attenuators were used to lower the laser power. The detectors were biased using a low noise DC power supply fed through a bias-tee. The RF signal coming from the devices was extracted using the bias-tee and amplified by a LNA with 2.4 dB noise figure, 2.5 GHz nominal bandwidth. The amplified signal was then acquired by a high-speed sampling oscilloscope with 1.7 ps jitter, Agilent 86100C, which directly measured and recorded delay, rise-time and jitter.

In order to quantify the high-speed transient response and corresponding high-speed parameters, the devices were illuminated with the pulsed laser at different attenuation levels. Under the illumination of the attenuated femtosecond laser, we were able to measure the response due to less than 5 photons at room temperature with averaging. The rise-time at 1 V bias was 200 ps with a jitter of 15 ps RMS. To see the effect of optical saturation, the power was increased to 14 pJ where the pulse shape started to exhibit compression. The compressed response was compared to the results without the LNA in the signal path to verify that the source of compression was indeed the nano-injection detector. Measurements of nominal RMS jitter with increased pulse intensity kept stable around 15 ps indicating that there was no significant change of the jitter.

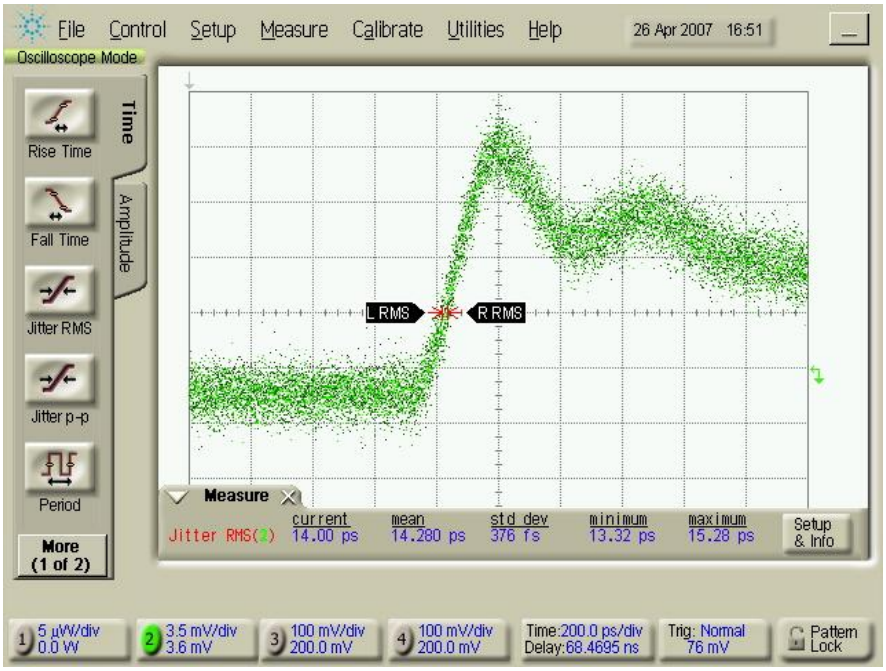

Fig. 5. The measured jitter of the devices was less than 15 ps RMS at room temperature.

The 2 µm laser spot was scanned using motorized drivers and a map of the delay around the device was extracted together with the amplitude of the response to evaluate the transit time. Measurements indicate that the active area of the device for pulsed illumination extended to 8-9 µm away from the nano-injectors. This was significantly less that the active area with CW illumination, which extended to beyond 100 µm, and we believe that the difference is due to a transient effect on the filling/emptying of surface states on the passivation interface.

The jitter performance was also re-evaluated using the measured delay and amplitude maps. A variable illumination spot size was assumed, and the spatial generation of carriers and corresponding transit delays were modeled and analyzed in MATLAB based on the delay maps. The expected jitter was calculated using the probability distribution for carrier arrival times. In parallel with the theorized delay-jitter relation and calculations, the laser was defocused to see and experimentally quantify the effect of spot size on jitter. The spot size was calculated using the deviation from the focal plane and the numerical aperture of the focusing lens. The results were in good agreement, except for small spot sizes, where the results are influenced by the saturation of the devices due to intense laser pulses very close to the nano-injectors. The saturation affects rising edge of the detector which, in turn, increased the effective delay. Hence, the close proximity of the injector exhibited a flat delay-vs-distance relationship and calculations with smaller spots showed less statistical distribution.

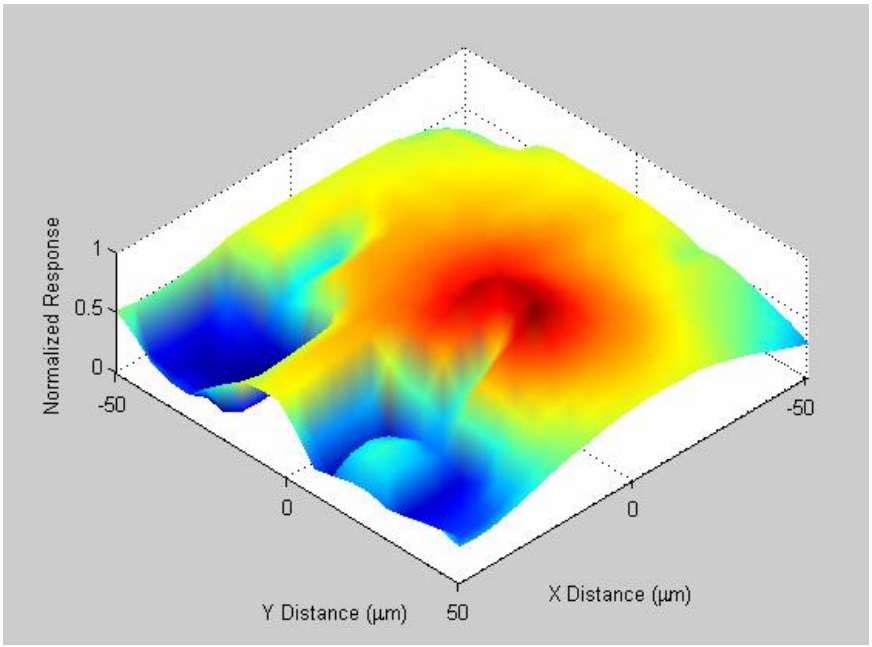

(a)

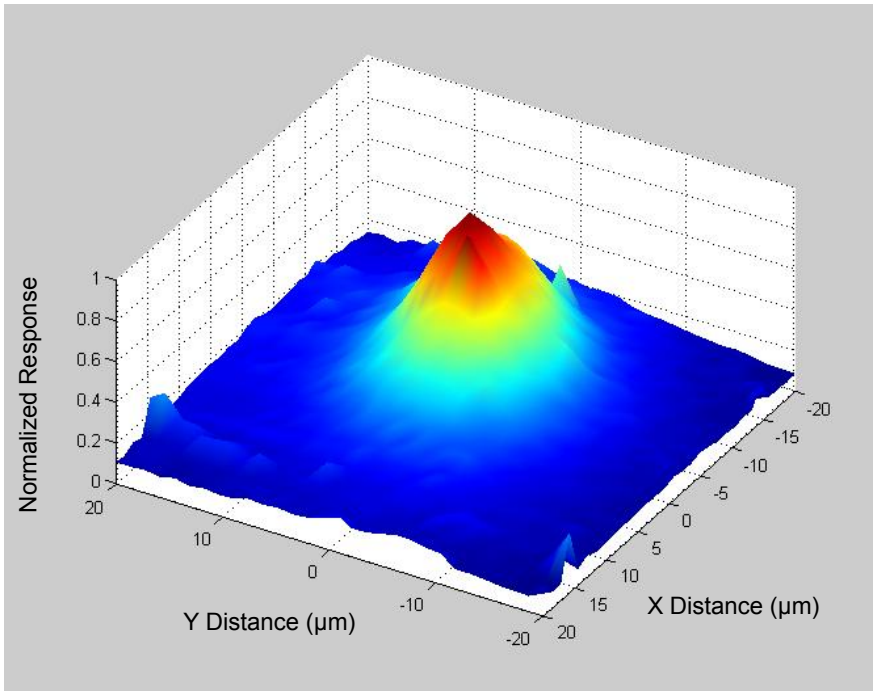

(b)

Fig. 6. (a) The spatial response of surface-passivated nano-injection detector under CW laser illumination, which extends beyond a diameter of 100 µm. (b) The spatial response of surface-passivated nano-injection detector under pulsed femtosecond laser illumination, which is localized to an area with a diameter of less than 20 µm.

4. CONCLUSION

We have presented a new approach towards short-wave infrared single photon imagers with the nano-injection detector. Designed to provide high performance in SWIR band, the nano-injection detector provides many desirable properties. Measurements on the first generation nano-injection devices have shown very high gain values, exceeding 10,000 and low dark current values. In parallel to the strong amplification, the devices exhibited high stability due to internal negative feedback. Related to the same internal feedback, suppressed shot noise levels were observed with Fano suppression factors as low as 0.55, which can be very beneficial in imaging arrays. The surface passivated arrays, suitable for read-out integrated circuit (ROIC) integration, showed high uniformity, with standard deviation less than 3%. The high uniformity of nano-injection detector would reduce, or even remove, the need for sophisticated pixel correction methods employed in ROICs. The surface passivated detectors also exhibited high speed response and very low timing jitter (<15 ps). These properties enable the nano-injection detectors to be utilized in high speed imaging using staring arrays.

REFERENCES

[1] P. Colarusso, L. H. Kidder, I. W. Levin, J. C. Fraser, J. F. Arens and E. N. Lewis, "Infrared Spectroscopic Imaging: From Planetary to Cellular Systems", Applied Spectroscopy 52, 104A (1998).

[2] J. Battaglia, R. Brubaker, M. Ettenberg and D. Malchow, "High speed Short Wave Infrared (SWIR) imaging and range gating cameras", Proc. of SPIE 6541, 654106 (2007).

[3] D.A. Fay, A.M. Waxman, M. Aguilar, D.B. Ireland, J.P. Racamato, W.D. Ross, W.W. Streilein, and M.I. Braunl, "Fusion of multi-sensor imagery for night vision: color visualization, target learning and search", Proceedings of the Third International Conference on Information Fusion, TuD3-3 (2000).

[4] M. H. Ettenberg, M. Blessinger, M. O'Grady, S.-C. Huang, R. M. Brubaker, and M. J. Cohen, "High-resolution SWIR arrays for imaging at night", Proc. of SPIE 5406, 46 (2004).

[5] P. Norton, "Third-generation sensors for night vision", Opto-Electronics Review 14, 1 (2006).

[6] A. Rogalski, "Optical detectors for focal plane arrays", Opto-Electronics Review 12, 221 (2004).

[7] M. Furumiya, H. Ohkubo, Y. Muramatsu, S. Kurosawa, F. Okamoto, Y. Fujimoto, Y. Nakashiba, Electron Devices, "High-sensitivity and no-crosstalk pixel technology for embedded CMOS image sensor ", IEEE Transactions on 48, 2221 (2001).

[8] R. S. Balcerak, J. Lupo, "Advances in infrared sensor technology and systems", EMBS/BMES Conference, Proceedings of the Second Joint, 1124 (2002).

[9] A. Poloczek, M. Weiss, S. Fedderwitz, A. Stoehr, W. Prost, D. Jaeger, and F. J. Tegude, "Integrated InGaAs pin-diode on exactly oriented silicon (001) substrate suitable for 10 Gbit/s digital applications", LEOS 2007, The 20th Annual Meeting of the IEEE, 180 (2007).

[10] S. Cova, M. Ghioni, A. Lotito, I. Rech, and F. Zappa, "Evolution and prospects for single-photon avalanche diodes and quenching circuits", J Mod Optic 51, 1267-1288 (2004).

[11] N. Duan, S. Wang, X. G. Zheng, X. Li, N. Li, J. C. Campbell, C. Wang, and L. A. Coldren, "Detrimental effect of impact ionization in the absorption region on the frequency response and excess noise performance of InGaAs/InAlAs SACM avalanche photodiodes", IEEE Journal of Quantum Electronics 41, 568 (2005).

[12] R. J. Mcintyre, "Multiplication noise in uniform avalanche diodes", IEEE Tran Electron Dev 13, 164 (1966).

[13] S. Somani, S. Kasapi, K. Wilsher, W. Lo, R. Sobolewski, and G. Gol'tsman, "New photon detector for device analysis: Superconducting single-photon detector based on a hot electron effect", J Vac Sci Technol B: Microelectronics and Nanometer Structures 19, 2766 (2001).

[14] O.G. Memis, A. Katsnelson, S. C. Kong, H. Mohseni, M. Yan, S. Zhang, T. Hossain, N. Jin, and I. Adesida, "A Photon Detector with Very High Gain at Low Bias and at Room Temperature", Appl Phys Lett 91, 171112 (2006).

[15] O.G. Memis, A. Katsnelson, S. C. Kong, H. Mohseni, M. Yan, S. Zhang, T. Hossain, N. Jin, and I. Adesida, "Sub-Poissonian Shot Noise of a High Internal Gain Injection Photon Detector", Optics Express, (Accepted for publication, 2008)

[16] O.G. Memis, A. Katsnelson, H. Mohseni, M. Yan, S. Zhang, T. Hossain, N. Jin, and I. Adesida, "On the Source of Jitter in a Room-Temperature Nanoinjection Photon Detector at 1.55 μm", IEEE Electron Device Letters 29, 867-869 (2008).
[17] S. Hecht, S. Shlaer, and M. H. Pirenne, "Energy, Quanta, And Vision", Journal of. Gen. Physioogy 25, 819 (1942).
[18] F. Rieke, and D. A. Baylor, "Single photon detection by rod cells of the retina", Reviews of Modern Physics 70, 1027 (1998).
[19] F. Z. Xie, D. Kuhl, E. H. Bottcher, S. Y. Ren, and D. Bimberg, "Excess noise measurement in avalanche photodiodes using a transimpedance amplifier front-end", J Appl Phys 73, 8641 (1993).
[20] V. Y. Aleshkin, L. Reggiani, N. V. Alkeev, V. E. Lyubchenko, C. N. Ironside, J. M. L. Figueiredo, and C. R. Stanley, "Giant suppression of shot noise in double barrier resonant diode: a signature of coherent transport", Semicond Sci Technol 18, L35 (2003).